

# Global bending quantum number and the absence of monodromy in the HCN↔CNH molecule

 K. Efstathiou,<sup>1</sup> M. Joyeux,<sup>2</sup> and D. A. Sadovskii<sup>1,\*</sup>
<sup>1</sup>Université du Littoral, UMR 8101 du CNRS, 59 140 Dunkerque, France

<sup>2</sup>Laboratoire de Spectrométrie Physique, Université Joseph Fourier–Grenoble I, UMR 5588 du CNRS, Boîte Postale 87, 38 402 St. Martin d’Hères, France

(Received 18 July 2003; published 23 March 2004)

We introduce and analyze a model system based on a deformation of a spherical pendulum that can be used to reproduce large amplitude bending vibrations of flexible triatomic molecules with two stable linear equilibria. On the basis of our model and the recent vibrational potential [J. Chem. Phys. **115**, 3706 (2001)], we analyze the HCN/CNH isomerizing molecule. We find that HCN/CNH has no monodromy and introduce the second global bending quantum number for this system at all energies where the potential is expected to work. We also show that LiNC/LiCN is a qualitatively different system with monodromy.

DOI: 10.1103/PhysRevA.69.032504

PACS number(s): 33.20.Vq, 45.50.-j, 03.65.Sq, 33.15.Mt

## I. INTRODUCTION

Action-angle variables play a central role in the description and analysis of internal dynamics of atomic and molecular systems. Such systems often have important integrable approximations for which these variables can be introduced. Particularly many approximations are obtained for the limit of small oscillations about an equilibrium or a periodic orbit. If the frequencies of oscillations are incommensurate, i.e., in the absence of resonances, such oscillators can be described very efficiently using a particularly simple and, arguably, the most popular version of action-angle variables and corresponding quantum numbers. Thus molecular vibrational Hamiltonians are commonly expanded in the so-called Dunham series in such action-angle variables.

In a general situation, actions  $I$  can be defined only *locally* as smooth real single-valued functions  $I(F)$  of the first integrals  $F$ , see Refs. [1–3] and Appendix D of Ref. [4]. Under certain general conditions these local actions  $I(F)$  can be extended to the whole domain of values of  $F$  [5]. However, different topological obstructions can make definition of such global actions *impossible* [6]. *Monodromy* is the simplest obstruction, it can be found in integrable systems with only two degrees of freedom.

After mathematicians provided several concrete examples of systems with monodromy, notably the *spherical pendulum* [7,8], physicists followed with discovery of monodromy in a number of fundamental atomic and molecular systems: the hydrogen atom in orthogonal (crossed) electric and magnetic fields [9], rotating molecules in external electric field [10], rotating linear triatomic molecules [11], systems with coupled angular momenta [12], and the  $H_2^+$  system [13]. Flexible or “floppy” triatomic molecules with linear equilibrium configuration is another candidate for a system with monodromy. In this paper we analyze HCN, one of the most studied such molecules. A brief mathematical introduction to monodromy can be found in Appendix A.

## A. Energy-momentum map $\mathcal{EM}$

We study a special simple case of two degree of freedom systems with axial symmetry  $SO(2)$ , such as the spherical pendulum and the pendular model of the HCN molecule. These systems can be described using two first integrals, *momentum*  $L$  corresponding to the  $SO(2)$  symmetry and *energy*  $H$ . The functions  $(L, H)$  define the *energy-momentum map*

$$\mathcal{EM}: \mathbb{R}^4 \rightarrow \mathbb{R}^2: (q, p) \rightarrow (L(q, p), H(q, p)) = (\ell, h).$$

As an example, consider the  $\mathcal{EM}$  map of the spherical pendulum, which we discuss later in Sec. II A. The image of this map is shown in Fig. 1, where the shaded area represents regular 2-tori. The joint spectrum of operators  $(\hat{L}, \hat{H})$  of the corresponding quantum system forms a lattice of points in the image of the  $\mathcal{EM}$  map, see Fig. 2.

## B. Monodromy

We like to understand how the fibers of our  $\mathcal{EM}$  fit together in the phase space. To this end we take a closed loop  $\Gamma$  in the domain of regular values of  $\mathcal{EM}$  (see Fig. 1), choose an initial point on  $\Gamma$  and define the coordinates on the corresponding  $\mathbb{T}^2$  fiber or the *period lattice* (see more in Appendix A 3 a). We redefine these coordinates continuously while moving along  $\Gamma$  and compare the final and the initial coordinate system after taking a tour on  $\Gamma$  thus finding the 2

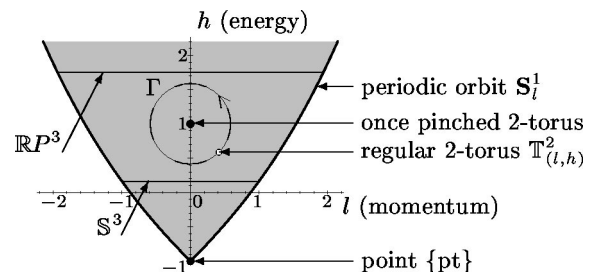


FIG. 1. Image and fibers of the energy-momentum map  $\mathcal{EM}$  of the spherical pendulum; see Chap. IV.3 of Ref. [4].

\*Electronic address: sadovski@univ-littoral.fr

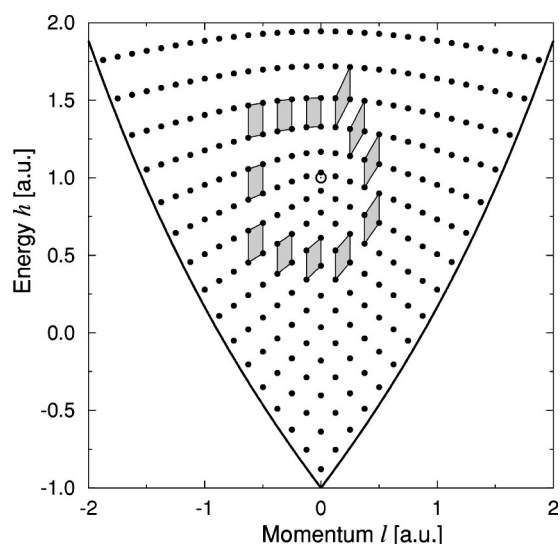


FIG. 2. Energy-momentum diagram for the spherical pendulum. Dots show quantum levels, bold solid lines represent relative equilibria, opaque circle marks the position  $(l, h) = (0, 1)$  of the unstable (“upper”) equilibrium. Rectangles show successive consistent definitions of local quantum numbers along the contour which goes around  $(0, 1)$ . Both axes are in atomic units but the quantization step is  $\hbar/8$ .

$\times 2$  monodromy matrix  $M$ . If the coordinate systems differ, i.e., if  $M$  is not unity, our system has monodromy and defining global action-angle variables and respective global quantum numbers (over the domain enclosed by  $\Gamma$ ) is impossible.

### C. Quantum lattice method

Using the local correspondence between the classical period lattice and the vectors defining the *elementary cell* of a sufficiently fine quantum  $\mathcal{EM}$  lattice (see Appendix A 2 c), we can replace continuation of period lattices for continuation of elementary cells. Since the cells are small, they can be easily extrapolated to the neighboring cells (see Appendix A 2 c, Fig. 15, right).

In particular, we can find *quantum monodromy* [8,14]. After completing a tour on  $\Gamma$  which we already used above, we compare now the vectors defining the initial and the final elementary cell and obtain the inverse transpose monodromy matrix  $(M^{-1})^\dagger$ . More generally, elementary cell continuation defines uniform quantum numbers for continuous families of states. If such definition can be expanded to the whole area of regular values of the  $\mathcal{EM}$ , then we talk of global quantum numbers.

Zhilinskií interpreted quantum monodromy as a *point defect* of the lattice of quantum states and developed the following simple method of the elementary cell diagrams which is similar to the methods used by crystallographers. We use this approach later throughout the paper. As an example we show in Fig. 2 how to find monodromy of the quantized spherical pendulum.

(1) Define the area  $D$  of interest in the image of the  $\mathcal{EM}$  map, possibly the whole image, and find singular values of  $\mathcal{EM}$ .

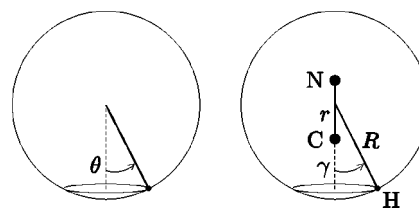


FIG. 3. Spherical pendulum (left) and flexible triatomic molecule HCN (right) with fixed bond lengths H-CN ( $R$ ), C-N ( $r$ ) and bending angle  $\gamma$ .

(2) Compute the joint quantum spectrum, i.e., the eigenvalues  $\langle \hat{L} \rangle$  and  $\langle \hat{H} \rangle$  of quantum operators  $\hat{L}$  and  $\hat{H}$ . If  $D$  is too small, reduce the value of  $\hbar$ .

(3) Take a closed contour  $\Gamma$  which passes the regular values of  $\mathcal{EM}$ , specify the direction of  $\Gamma$ .

(4) Take the initial-final point  $\gamma_0 = \gamma_1$  on  $\Gamma$ , define the elementary cell at  $\gamma_0$ .

(5) While moving along  $\Gamma$  in small steps, follow the continuous evolution of the cell (cf. Fig. 15, right).

(6) After making a tour, compare the final and the initial cell and find the monodromy matrix.

In this simple form the elementary cell method is ready for the coming revisions of undergraduate quantum-mechanics courses. Despite its simplicity the method is mathematically rigorous: relation between the period lattices and elementary cells becomes exact in the limit of  $\hbar \rightarrow 0$  (when the cells become infinitesimal) and using the Einstein-Kramers-Brillouin (EBK) quantization techniques we can work analytically. At the same time, we have a very rapid and efficient way of study of real molecular systems where numerical computations are unavoidable.

## II. PENDULUM MODELS OF FLEXIBLE TRIATOMIC MOLECULES

Spherical pendulum can be represented as a motion of a particle (of mass  $m$ ) constrained to a sphere (of radius  $R$ ) and placed in a linear gravitational field (directed conventionally along the vertical axis), see Fig. 3. This is very similar to the isomerizing HAB/ABH system, where the proton H can go around the diatom fragment AB. Like the spherical pendulum, the molecular system has axial symmetry and two linear (i.e., axially symmetric) equilibrium configurations HAB and ABH.

### A. Monodromy of spherical pendulum

On the example of spherical pendulum, we introduce relative equilibria, energy-momentum map, monodromy. Details can be found in Appendix B.

#### 1. Fibers of the $\mathcal{EM}$ map, monodromy

The image of the  $\mathcal{EM}$  map of the spherical pendulum is shown in Fig. 1. The domain  $A$  of regular values (shaded area) is bounded from below. The critical point  $(\ell, h) = (0, -1)$  corresponds to the stable (“lower”) equilibrium point of

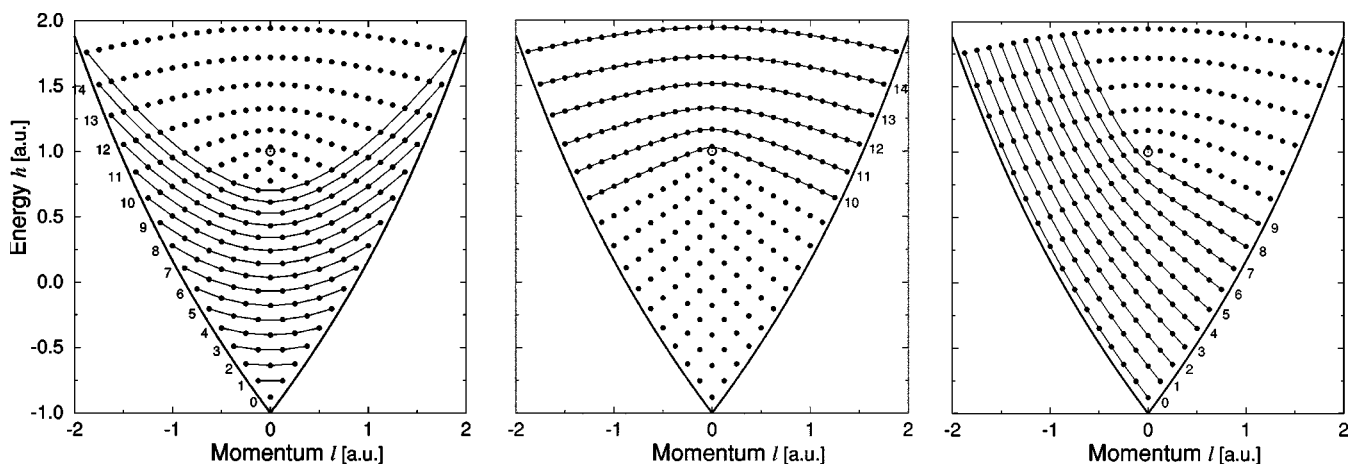


FIG. 4. Possible choices of quantum numbers for the spherical pendulum (left to right): “vibrational”  $n$ , “rotational”  $j$ , and “mixed”  $n+l$ ; cf. Fig. 2. Fine solid lines join states with the same quantum number which is given at the end of the sequence.

the system; other points in the boundary correspond to relative equilibria, see Appendix B 1 for more details.

We are primarily interested in the other critical value  $(0, 1)$ . This value is isolated within  $A$  and lifts to a *pinched torus* whose pinch point is the unstable (“upper”) equilibrium. Consequently, the system has monodromy 1 (see Appendix A 3 b). Quantum energies of the spherical pendulum can be computed in the standard way, see Appendix B 4. Figure 2 presents the resulting lattice of quantum states and illustrates quantum monodromy  $\begin{pmatrix} 1 & 0 \\ 1 & 1 \end{pmatrix}$  of the system.

## 2. Quantum numbers

Monodromy prevents defining the global second quantum number for the entire lattice of quantum states of the spherical pendulum system. Using the elementary cell continuation method in Sec. I C, we can of course define smooth sequences of states, but we will fail when we try to extend them to the whole lattice. This is illustrated in Fig. 4.

In particular, the vibrational quantum number  $n$  works correctly near the dynamical limit of the 1:1 resonant oscillator for  $h \approx -1$  (cf. Appendix B 1 c). Above the stable equilibrium with  $\ell=0$  and  $h=-1$ , we see constant  $-n$  multiplets or *polyads* of  $n+1$  levels whose energy is also nearly constant (Fig. 4, left). Note that levels with even (odd) value of  $\ell$  belong to even (odd)  $n$  polyads. The values of  $\ell$  within a polyad go by two so that  $|\ell|=n, n-2, \dots, 0$  when  $n$  is even and  $|\ell|=n, n-2, \dots, 1$  when  $n$  is odd. Due to this latter property the points of the lattice near  $(\ell=0, h=-1)$  form a checkerboard pattern. In order to apply the elementary cell technique in Sec. I C in terms of quantum numbers  $n$  and  $\ell$  we should choose a “double” cell with  $\Delta\ell=\Delta n=2$ .

Similarly, near the dynamical limit of free rigid spherical rotor where  $h \gg 1$ , the rotational quantum number  $j$  is a natural choice (Fig. 4, center). In this region we can see  $j$  multiplets with  $2j+1$  levels of nearly the same energy. The values of  $\ell$  go simply as  $|\ell|=j, j-1, \dots, 0$ ; the lattice has a straightforward rectangular pattern and we can define a single cell with  $\Delta\ell=\Delta j=1$  for extending the local quantum number definition and monodromy computation.

These two choices are widely used in analogous molecular systems [10,15]. In the case of the spherical pendulum, neither can be continued beyond the transition energy region of  $h \approx 1$  if we want our quantum numbers to be extrapolated by *smooth functions* of  $(\ell, h)$ , a necessary requirement for physically meaningful global quantum numbers. Of course, as a matter of convenience all wave functions can be labeled continuously using  $j$  (or  $n$ ) if the labels are chosen differently for  $l > 0$  and  $l < 0$ . The energy of the states in the resulting multiplets does not depend smoothly on such labels and exhibits the so-called “kink” [15]. The kink occurs if we formally continue  $j$  multiplets to  $h < 1$  as shown in Fig. 4, center. Same happens to  $n$  polyads as we try going above  $h=1$ . Such  $|\ell|$ -like behavior should not be attributed directly to monodromy but rather to the particular labeling system of quantum solutions.

## B. Flexible molecules as pendula

Without translations the total number of degrees of freedom of the isomerizing triatomic molecule, such as HCN/CNH, is six. The pendulum model in Fig. 3 deals with only two of these degrees. Molecular physicists like describing these pendular degrees as “bending” using the bending angle  $\gamma$  (see Fig. 3 and Appendix B 2 a) and “rotation” about the axis of the CN diatom using the angular momentum  $\ell$ . The other four degrees of freedom are the two stretching modes described by distances  $r$  between C and N and  $R$  between H and CN (see Fig. 3) and rotations of the molecule as a whole about axes which are roughly orthogonal to the CN axis. These extra degrees present, obviously, the major difficulty.

The order-of-magnitude difference of masses  $m_H$  and  $m_{CN}$  and the relative rigidity of the CN bond make it possible to consider an approximate separation of the two degrees of freedom associated with the overall rotation. Ignoring these two degrees, and assuming constant bond distances  $R$  and  $r$ , as shown in Fig. 3, right, makes HCN a good candidate system for a “molecular spherical pendulum.”

The most obvious difference between the spherical pendulum and molecules is the potential  $V$ . For the spherical



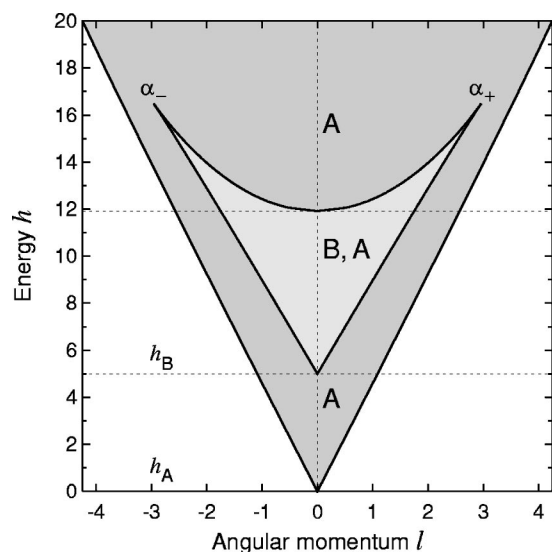


FIG. 5. Image of the classical energy-momentum map (light and dark shaded area) for the quadratic spherical pendulum defined in Sec. II C.

pendulum  $V=z$ , the lower equilibrium is stable and the upper equilibrium is unstable. In molecules  $V$  is more complicated. In particular, *both* linear equilibria of HCN/CNH are stable. In order to account for such qualitative difference we deform the potential of the spherical pendulum and show in Sec. II C and Appendix B 1 a that the deformed system with two stable linear equilibria and one new unstable “bent” equilibrium still has monodromy. The other important difference is the “shape” of the system. While in the spherical pendulum  $R$  is fixed and the particle moves on a sphere, in the HCN/CNH molecule  $R$  depends *considerably* on the bending angle  $\gamma$  and  $H$  moves on a deformed sphere. We study the influence of the shape on monodromy in Sec. II D and Appendix B 3.

The looseness of the bond between H and CN results not only in the shape effect, which modifies the kinetic energy of the pendulum system, but has further dynamic consequences of coupling the large amplitude bending motion of the pendulum and the oscillation of the pendulum length  $R$ . If the frequency of this latter is in a low-order resonance with the pendular frequency, the stretching and bending degrees of freedom are inseparable. The empiric rule is that the bending-to-stretching frequency ratio is about  $\frac{1}{2}$ , as in the most known example of the Fermi resonance in  $\text{CO}_2$ . The same resonance is very important in many flexible molecules, in particular, in HCP and HClO. Such systems cannot be analyzed on the basis of the pendulum model. On the other hand, HCN/CNH has no strong resonance (Sec. III) and this system can indeed be analyzed using an appropriately deformed spherical pendulum.

### C. Quadratic deformation of spherical pendulum

We deform the spherical pendulum by replacing the potential term  $z$  in Eq. (B1) for a quadratic potential

$$V(z) = c_1 z - \frac{1}{2} c_2 z^2 + c_0, \quad (1)$$

so that both linear equilibria of this system are now stable. We call  $A$  the lower ( $z=-1$ ) and  $B$  the upper ( $z=1$ ) equilibrium. Their energies are

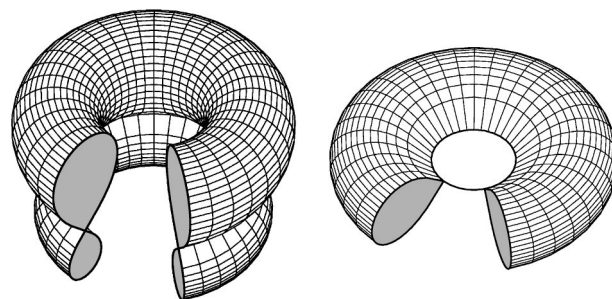


FIG. 6. Inverse images of the points in the upper boundary  $[\alpha_-, \alpha_+]$  of leaf  $B$  of the  $\mathcal{EM}$  map image of the quadratic spherical pendulum in Fig. 5.

$$h_A = c_0 - \frac{1}{2} c_2 - c_1 = 0, \quad h_B = c_0 - \frac{1}{2} c_2 + c_1,$$

where parameters can be chosen to mimic the HCN/CNH system so that  $A$  and  $B$  correspond to HCN and CNH,

$$c_0 = c_1 + \frac{1}{2} c_2, \quad c_1 = 2.5, \quad c_2 = 18.5.$$

Relative equilibria and other singular fibers of the  $\mathcal{EM}$  map of this new system can be analyzed in the same way as for the original spherical pendulum, see Appendix B for details. The image of the  $\mathcal{EM}$  map has now *two* leaves. Our particular example with  $h_A < h_B$  is illustrated in Fig. 5. In this figure, the larger leaf  $A$  represents both the vibrational states localized near the  $A$  minimum and rotational (delocalized) states, while the smaller leaf  $B$  represents vibrational states localized near the  $B$  minimum. The leaves  $A$  and  $B$  are glued along the segment  $[\alpha_-, \alpha_+]$  of singular values of  $\mathcal{EM}$  which lies entirely inside  $A$ . Note that  $B$  and  $A$  overlap in the image of the  $\mathcal{EM}$  map so that  $B$  looks like an “island.” The points in  $(\alpha_-, \alpha_+)$  lift to the singular fiber which has the topology of two cusped tori glued along their cusped principal circle, see Fig. 6, left; the cusp points  $\alpha_\pm$  correspond to a “cusped torus” in Fig. 6, right. Points on the lower boundaries of leaves  $A$  and  $B$  represent relative equilibria (cf. Sec. II A 1); the two singular apices of these boundaries at  $l=0$  correspond, of course, to the stable equilibrium points.

The singular segment  $[\alpha_-, \alpha_+]$  exists for  $c_2 > c_1 > 0$ ; when  $c_2 \rightarrow c_1 > 0$ , it shrinks to a point. The  $\mathcal{EM}$  map of the system with  $0 < c_2 < c_1$  is qualitatively the same as that of the spherical pendulum with  $c_2=0$ . Such system has the same monodromy as the spherical pendulum.

It is clear that a slightly deformed system with  $c_2$  just above  $c_1$  also has the same monodromy. To find this monodromy we should make a tour along a contour  $\Gamma$  which lies in the leaf  $A$  and goes around  $[\alpha_-, \alpha_+]$ . The quantum lattice  $A$  will therefore have a segment defect in place of a point defect as illustrated in Fig. 7. Note that in Fig. 7 we should well distinguish points of the  $A$  lattice (filled circles) from those of the  $B$  lattice (empty circles) in order to continue the elementary cell of the  $A$  lattice in the overlap region of the  $\mathcal{EM}$  image. The cell can, obviously, be continued using only the  $A$  points. (In classical terms, we should remain on the  $A$  leaf.) The lattices  $A$  and  $B$  join along the segment but there is no passage between them, in the sense that we cannot define

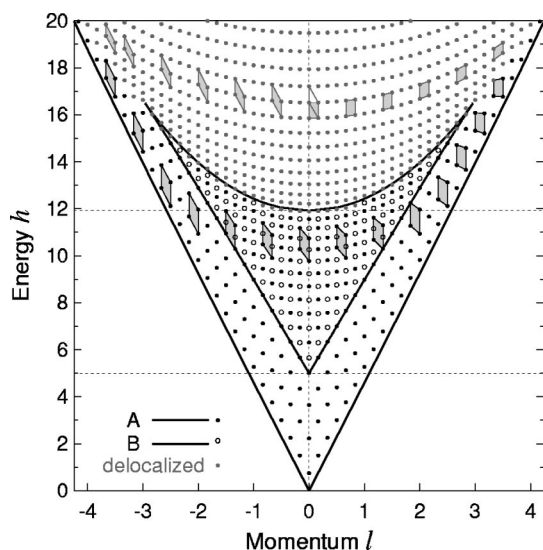


FIG. 7. Quantum and classical energy-momentum diagram for the quadratic spherical pendulum defined in Sec. II C. Rectangles show successive consistent definitions of local quantum numbers along the contour which goes around the line of singular values of the main leaf A, cf. Fig. 5. Both axes are in atomic units but the quantization step is  $\hbar/8$ .

the second smooth global action and corresponding quantum number to label uniformly the quantum states in the two lattices; neither can we define such global action and quantum number for the A lattice. Our main question is whether the quantum states of the real HCN/CNH system are organized in the similar fashion and specifically, whether this system has monodromy.

#### D. Shape correction

In flexible molecules such as HCN/CNH or LiNC/NCLi, the distance  $R$  tends to be smaller in the  $\perp$  configuration when  $\gamma \approx \frac{1}{2}\pi$ . We can model this by using

$$R(\gamma) = R_0(1 - \epsilon \sin^2 \gamma), \quad (2)$$

where  $1 > \epsilon > 0$  is the *asphericity parameter*. Of course, any such deformation of the spherical shape of the pendulum complicates the expression for the kinetic energy. For relative equilibria, however, the modification is straightforward. The concrete computation in Appendix B 3 for the shape (2) shows that at small asphericity  $\epsilon < \frac{1}{3}$  the  $\mathcal{EM}$  diagram of the system is qualitatively the same as that in Fig. 7. For larger  $\epsilon$  the shape is no longer convex and this modifies qualitatively the  $\mathcal{EM}$  diagram (see Fig. 8): the cusp points  $\alpha_{\pm}$  disappear and the singular segment becomes a line of singular values.

Comparing to the small asphericity case in Sec. II C and Fig. 5, we see that we now have *three* leaves which we denote by  $A'$  for oscillations localized near the A minimum,  $B$  for the oscillations localized near the B minimum, and  $A''$  for the delocalized bending motion. The leaves are glued along their common boundary which is the upper boundary of  $B$  and  $A'$  and the lower boundary of  $A''$ . As before,  $A'$  and  $B$  overlap in the image of  $\mathcal{EM}$ . All leaves are unbounded from above. All fibers remain the same as in the case of

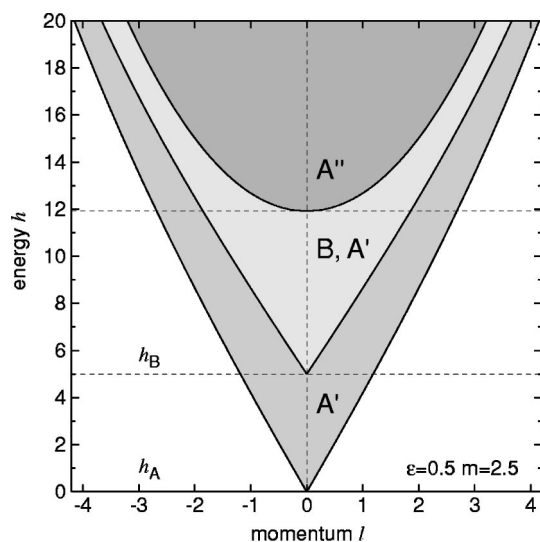


FIG. 8. Image of the classical energy-momentum map (shaded areas) of the quadratic aspherical pendulum with asphericity  $\epsilon = \frac{1}{2}$  and quadratic potential constants  $c_0, c_1, c_2$  used in Sec. II C; cf. Figs. 5 and 10.

small  $\epsilon$  except, of course, for the two “cusped tori” which disappear. Since there is no longer a finite segment about which our elementary cell can make a tour, such nonconvex system has no monodromy.

### III. GLOBAL BENDING QUANTUM NUMBERS AND ACTIONS IN HCN

Analysis of the early energy surfaces of the isomerizing HCN/CNH system [16,17] shows that this system is somewhat exceptional: it has no prominent low-order stretching-bending resonance. Consequently, we can average over the oscillations of  $R$  and  $r$  and obtain a pendulumlike reduced system. More concretely, we decouple the two stretching degrees of freedom of HCN/CNH from the pendular motion by applying canonical perturbation theory to a reaction path Hamiltonian. A classical version of this procedure was developed in Refs. [18,19]. We use the quantum procedure described in Ref. [20], where the improvement over [18,19] is in correct handling of vibrational angular momentum for large values of  $\ell$ .

The starting point of our present calculations is the most recent *ab initio* potential-energy surface of HCN/CNH by Tennyson and co-workers [21,22]. According to this surface, the CNH linear equilibrium configuration is located at about  $5300 \text{ cm}^{-1}$  above the HCN linear equilibrium configuration and the two equilibria are separated by a barrier at about  $16\,800 \text{ cm}^{-1}$ , see Fig. 9, bottom. This potential is qualitatively similar to the quadratic potential in Sec. II C. Figure 9 also shows the variation of  $r$  and  $R$  along the minimum energy path (MEP) for the potential [21]. We find that in good agreement with our intuitive model of the rigid CN diatom (Sec. II B) the CN distance  $r$  changes negligibly. At the same time,  $R$  decreases significantly in the  $\perp$  configuration. As a result, H moves on a peanutlike *nonconvex* surface.

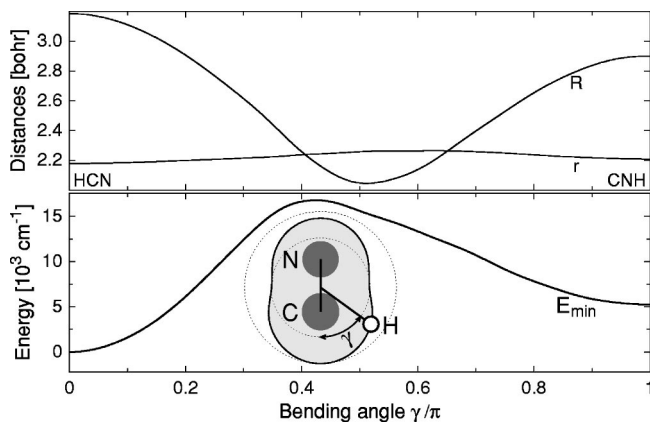


FIG. 9. Geometry and reaction path minimum potential energy of the HCN/CNH system computed for the *ab initio* potential surface in Refs. [21,22]. Atoms C, N, and H are sized according to their covalent radii.

### 1. Reduced effective Hamiltonian

Following Refs. [18,19], the potential and kinetic energies of the system are first expanded in the neighborhood of the reaction path (or MEP), which leads from HCN to CNH through the saddle; the two stretch coordinates are defined as deviations  $r - r_{\text{MEP}}(\gamma)$  and  $R - R_{\text{MEP}}(\gamma)$  from their values on the MEP and then rescaled to obtain the dimensionless normal stretch coordinates. The expansion is rewritten in terms of these coordinates. The principal virtues of this expansion are (i) the optimal representation of the coupling between stretching and pendular modes with only few truly pertinent relatively small explicit coupling terms and (ii) the simplification of the Hamiltonian, which contains only powers of the stretch coordinates, conjugate momenta, harmonics of the bending angle  $\gamma$ , and the momentum conjugate to  $\gamma$ .

The second step of the procedure consists of several canonical transformations which are aimed at separating the stretching motion completely and introducing the two stretch quantum numbers (or corresponding two classical oscillator actions) as parameters. This results in an effective quantum Hamiltonian of the form

$$\hat{H}_\ell(n_1, n_3, J, \gamma) = \sum_{i,j} \sum_{k,m,p} a_{i,j,k,m,p} n_1^i n_3^j \cos^k \gamma \left( \sin \gamma \frac{\partial}{\partial \gamma} \right)^p (\hat{J}^2)^m, \quad (3)$$

where coefficients  $a_{i,j,k,m,p}$  are real,  $n_1$  and  $n_3$  are the  $R$  and  $r$  stretch quantum numbers respectively,  $\gamma$  is the bending angle in Fig. 3, the exponent  $p$  is either 0 or 1,  $\hat{J}^2$  is defined in Eq. (B8) with  $\theta = \gamma$ , and  $\ell$  is called the quantum number of the vibrational angular momentum. In this work, we computed  $\hat{H}_\ell$  in Eq. (3) after six successive transformations, its coefficients  $a_{i,j,k,m,p}$  can be obtained by contacting the authors.

### 2. Energy-momentum map $\mathcal{EM}$

The classical Hamiltonian can be obtained from the quantum expression in Eq. (3) by discarding the terms with  $p$

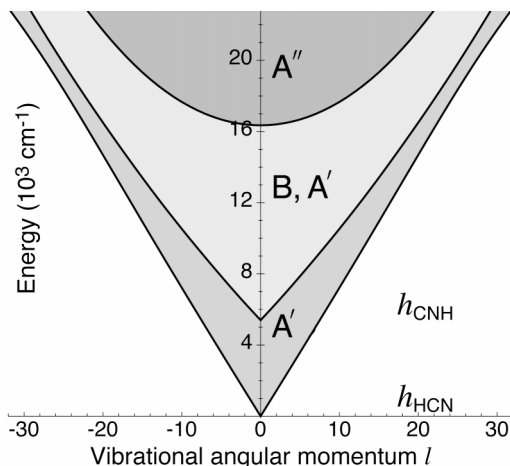


FIG. 10. Image of the energy-momentum map (shaded areas) of the isomerizing HCN/CNH system computed for pure bending states with  $\nu_1 = \nu_3 = 0$  using the classical analog of the Hamiltonian (3).

$= 1$ , which originate from the noncommutativity of  $\cos^k \gamma$  and the differential operators in Eq. (3), and by replacing  $\hat{J}^2$  by its classical analog in Eq. (B5). The image of the  $\mathcal{EM}$  map of the HCN/CNH system is shown in Fig. 10 for the pure bending states with  $\nu_1 = \nu_3 = 0$ ; very similar plots are obtained for other values of  $\nu_1$  and  $\nu_3$ . As predicted in Sec. II D for nonconvex systems, this image is qualitatively the same as that of the largely aspherical quadratic pendulum in Fig. 8. We conclude that HCN/CNH has no monodromy.

### 3. Computing quantum energies

Quantum energy spectrum of the reduced Hamiltonian  $\hat{H}_\ell$  in Eq. (3) is computed as before (see Appendix B 4). The advantage of using  $\hat{H}_\ell$  over the full initial Hamiltonian in Ref. [22] is in the predefined value of the global quantum number  $\ell = 0, 1, 2, \dots$ . The resulting lattice of quantum states is shown Fig. 11.

In order to check the accuracy of our pendular approximation we compare our energies of the  $\ell = 0$  states localized in the HCN and CNH wells, called vibrational *band origins*, to the values in Tables VI and VII of Ref. [21]. We reproduce the 101 origins, which go all the way up to the isomerization threshold and have up to 18 quanta of excitation in the bending mode, with an average error of  $10.4 \text{ cm}^{-1}$  and a maximum error of  $38.3 \text{ cm}^{-1}$ . Furthermore, as can be seen in Fig. 11, we also reproduce satisfactorily the energies for  $\ell \neq 0$ . An even better agreement could be obtained by taking into account the kinetic-energy terms which are responsible for the  $\ell^2$  anharmonic correction in the effective Hamiltonian.

### 4. Defining the second global quantum number

First of all we should specify the kind of the global quantum number (classical action) which we look for. Normally, global actions are defined over one open connected domain in the image of the  $\mathcal{EM}$  map. We have three domains  $A'$ ,  $A''$ , and  $B$ . So we should first attempt to define the second action globally within each of the domains. (Remember that in the



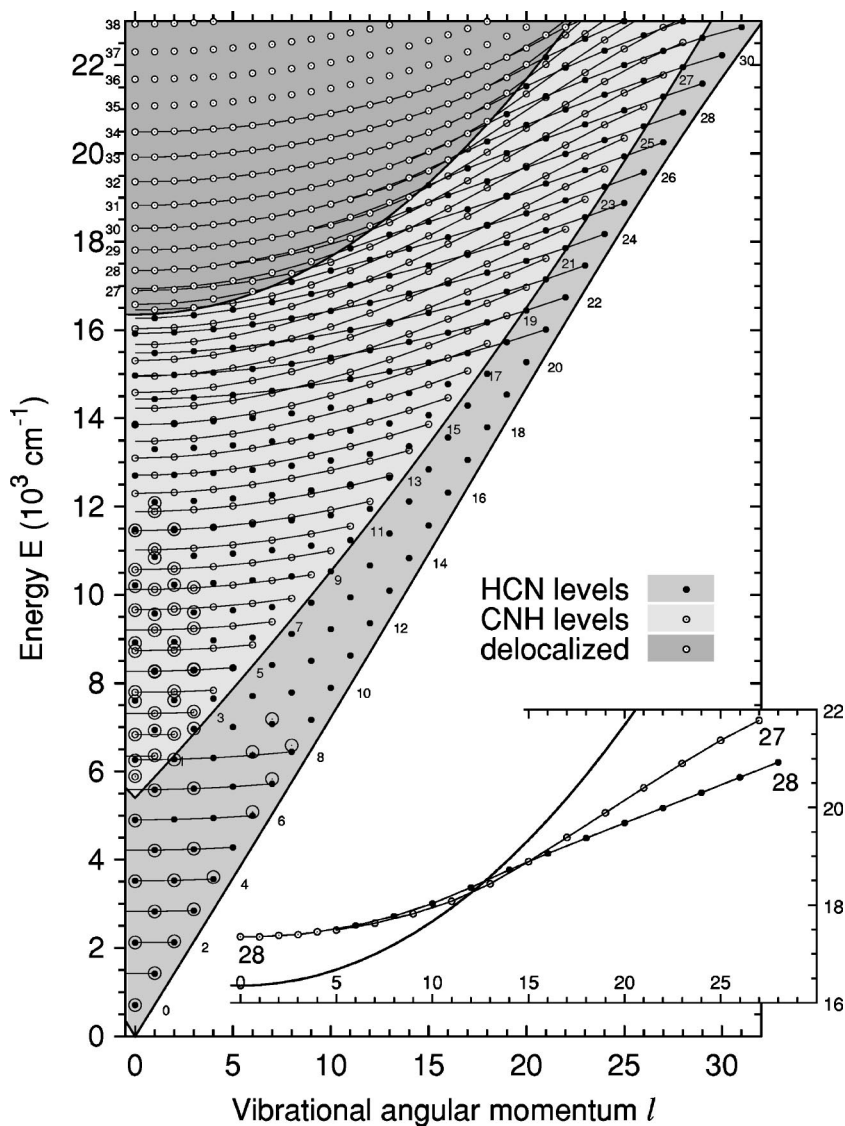


FIG. 11. Energy-momentum diagram for the  $\nu_1 = \nu_3 = 0$  states of the HCN/CNH system computed using the Hamiltonian (3). Shades of gray distinguish HCN, CNH, and delocalized level regions respectively, cf. Fig. 10. The regions are bordered by the energies of classical relative equilibria shown by bold solid lines. Filled circles show levels attributed to the HCN minimums while hollow circles represent either CNH or delocalized states depending on the region. A few larger black circles mark levels assigned in Ref. [22]. Fine solid lines join states with the same quantum numbers  $n_{\text{HCN}}$ ,  $n_{\text{CNH}}$ , or  $j$ , whose values are given at the end of the respective sequences. The diagram is symmetric with respect to  $\ell \leftrightarrow -\ell$ , and only half of it is shown.

model  $\epsilon < \frac{1}{3}$  system in Sec. II C this was not possible for the leaf A due to monodromy.) If succeeded, we can try relating these actions in order to define one unique generalized global action and the corresponding quantum number. This generalized action is a real function  $\mathcal{F}(q, p)$  which is two valued in the overlap region of  $A'$  and  $B$ , and single valued in  $A''$ . The branching of the values of  $\mathcal{F}$  should correspond to the branching of  $A''$  into the leaves  $A'$  and  $B$ . The image of the  $\mathcal{EM}$  map serves similarly to Riemann surfaces in complex analysis.

We now define quantum numbers in each domain. The natural choice of these numbers is already considered for the spherical pendulum in Sec. II A 2. We will use two vibrational numbers  $n_{\text{HCN}}$  and  $n_{\text{CNH}}$  in domains  $A'$  and  $B$ , respectively, and rotational number  $j$  in domain  $A''$ . In Fig. 11 we connect levels in the same  $n$  polyad and  $j$  multiplet by one line.

Vibrational polyads are clearly seen in Fig. 11 at the bottom of leaves  $A'$  and  $B$ . At low energies, the levels in these polyads are practically degenerate (in the scale of Fig. 11). The polyad numbers can be given an absolute value starting with the ground state ( $n=0, \ell=0$ ) at the bottom of each leaf.

With growing energy and  $n$ , the relative energy of the high  $\ell$  end of the polyads increases. Above  $h \approx 16000 \text{ cm}^{-1}$  where all three domains overlap in energy, the polyads cannot be completed to  $n+1$  levels (lattice points), only their high  $\ell$  ends still exist. This is well seen in Fig. 11 where the fine lines connecting levels in the same polyad begin crossing (from right to left) the singular value line which gives the common boundary of  $A'$ ,  $A''$ , and  $B$ .

Rotational quantum number  $j$  cannot be defined absolutely because the multiplets are incomplete (at least within the energy range of Fig. 11). Starting at small  $\ell$  and using our elementary cell approach in Sec. I C we can only assemble some levels in rotational multiplets and extend our definition over the whole domain  $A''$ ; our lines representing multiplets cross inevitably over the lower boundary of  $A''$ , see Fig. 11.

*The main result of this paper is that the three lattices of quantum states can be connected and that the connection is likely to be smooth.* Figure 11 shows how for each rotational multiplet we find the two corresponding vibrational polyads with labels  $n_{\text{HCN}}$  and  $n_{\text{CNH}}$ , and define the global bending number

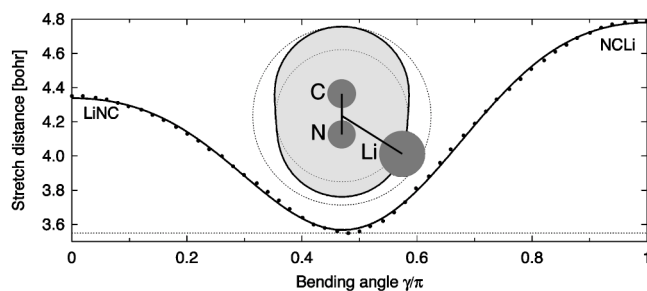


FIG. 12. Minimum stretch distance  $R$  in the LiNC-NCLi system computed for the *ab initio* potential in Ref. [24].

$$\mathcal{J} = j = n_{\text{HCN}} = n_{\text{CNH}} + 1,$$

i.e.,  $\mathcal{J} = j$  on leaf  $A''$ ,  $\mathcal{J} = n_{\text{HCN}}$  on leaf  $A'$ , and  $\mathcal{J} = n_{\text{CNH}} + 1$  on leaf  $B$ , so that the full three-branch  $\mathcal{J}$  multiplet contains  $2\mathcal{J} + 1$  levels, see the example of  $\mathcal{J} = j = n_{\text{HCN}} = 28$  and  $n_{\text{CNH}} = 27$  in Fig. 11. Note that the elementary cell continuation in the region near the common boundary of the three leaves is difficult because quantum states in this region are irregular and cannot be attributed with certainty to any of the leaves. To reduce this difficulty, recall that levels in the  $n$  polyads step by 2, while  $j$  multiplets contain states with both odd and even  $\ell$  (see Sec. II A 2). This means that if we want to connect two incomplete polyads with quantum numbers  $n_{\text{HCN}}$  and  $n_{\text{CNH}}$  to a  $j$  multiplet, the numbers  $n_{\text{HCN}}$  and  $n_{\text{CNH}}$  should be of different parity and, if we want the connected multiplet to be complete, these numbers should differ by 1. Then only two possibilities are left, and the one we found is more logical in view that the HCN minimum lies below the CNH one.

#### IV. MONODROMY IN LiNC

We have seen in Secs. III and II D that the anticipated monodromy phenomenon is prevented in HCN/CNH by the “excessive” asphericity of the system. In fact we have missed this phenomenon in HCN by a small margin: a rough estimate for asphericity gives  $\epsilon \approx (R_{\text{max}} - R_{\text{min}})/R_{\text{max}} = 0.36$ . It follows that we should look for a similar system with smaller asphericity such as the LiNC/NCLi molecule [23]. The  $(R, \gamma)$  potential surface of LiNC/NCLi was obtained in Ref. [24] for the C-N distance fixed at  $r = 2.186$  bohr. According to Ref. [24] the LiNC equilibrium is the lowest in energy. Like in HCN/CNH, both linear equilibria of LiNC/NCLi are stable and there is no strong resonance between stretching and bending. More importantly, since Li is much larger than H, it stays at larger distances  $R$  and the system remains *convex*, see Fig. 12. The same asphericity estimate now gives  $\epsilon \approx 0.25$ .

We treated LiNC/NCLi in the same way as HCN/CNH using sixth-order canonical perturbation theory. Since  $r$  was fixed in Ref. [24], we only had to normalize over the Li-NC vibration and define the respective quantum number. Our computed band origins are in good agreement with the  $J=0$  levels in the full quantum calculation of Ref. [25]. The energy-momentum diagram for the pure bending states (without excitation of the stretching degree of freedom  $R$ ) of

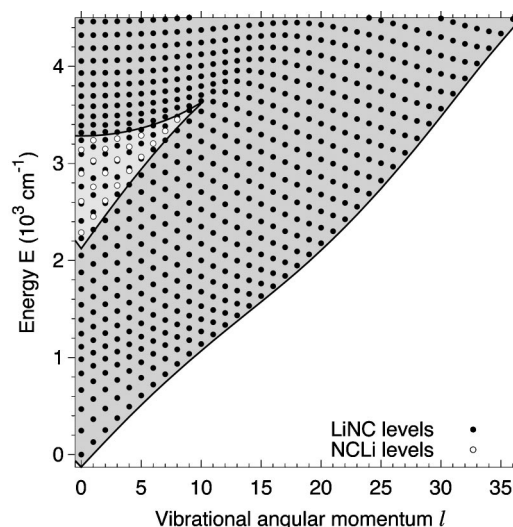


FIG. 13. Energy-momentum diagram for the pure bending states of LiNC/NCLi computed using the *ab initio* potential in Ref. [24]. Hollow circles show levels attributed to the NCLi minimum; filled circles represent LiNC levels which become delocalized states at higher energies; bold solid lines show energies of classical relative equilibria. The diagram is symmetric with respect to  $\ell \leftrightarrow -\ell$  and only half of it is shown.

LiNC/NCLi is shown in Fig. 13. Comparing to Fig. 7 we conclude that in full agreement with our prediction in Sec. II D for the case of small  $\epsilon$ , this system has monodromy of the kind described in Sec. II C.

#### V. DISCUSSION

The study of obstructions to global action-angle variables in molecular and atomic systems remains still at a descriptive stage and is of interest to a limited community of mathematicians and theoretically motivated physicists. Yet the potential importance of this study to a much wider audience should be recognized. After several important physical systems with monodromy have been found, our next question is naturally: What is the principal difference of systems with global angle-action variables, and systems with monodromy, and how can we manifest or “exploit” this difference? This question remains open. The answer involves expertise in several fields, such as modern semiclassical theories, wave-packet techniques and corresponding experiments, geometric phase theory, and others.

##### A. Results

Our present concrete study allows to state a likely proposition that the HCN/CNH molecular system without rotation can be described in terms of global quantum numbers and therefore has no monodromy. This should bring certain satisfaction to theoretical chemists and spectroscopists, who have been for a long time using bending quantum numbers for the assignment of the energy levels of HCN/CNH. The absence of monodromy makes HCN/CNH qualitatively different from the LiNC/NCLi system which has monodromy. The reason for this difference is the nonconvex shape of HCN/CNH, see Figs. 9 and 12.



**B. Limitations**

We considered a subsystem of four internal degrees of freedom of the isomerizing triatomic molecules HCN and LiNC (Sec. II B). Extending our results to the complete system depends on whether the two excluded degrees related to the overall rotations of the molecule can be effectively separated. Two aspects are of major concern in this context: the ratio of the energy of such rotations to that of the bending oscillations, and the dependence of the instantaneous inertia tensor  $\mathcal{I}$  on the position of H or Li. Since Li is heavier and moves at larger distances from the CN diatom than H, the two systems differ substantially in both aspects and should be examined individually. Thus the contribution of H to  $\mathcal{I}$  does not exceed 15 % and we can distinguish rotations of HCN/CNH about axes roughly orthogonal to the CN axis. This is clearly not the case for LiNC/CNLi.

In LiNC/NCLi we could not account for the N-C stretch which was frozen in the potential [24]. This is justifiable in general because the ratio of the frequency of this vibration to that of the bending mode is about 15:1. However, this frequency is close to the energies of the NCLi states in which we are interested.

In HCN/CNH we do not prove the smoothness of the junction of the two families of high- $\ell$  vibrational bending states and the rotational multiplet. We should further study this analytically for the strongly aspherical quadratic pendulum model (Sec. II D). More importantly, we cannot extrapolate to energies much higher than shown in Figs. 10 and 11 which cover all energies where the potential [21,22] is believed to work, and by far all experimentally studied states of HCN/CNH.

**C. Perspectives**

On the technical side, further analysis should begin with the development of consistent classical mechanical description of flexible molecules which is similar to the polar-coordinate-free study of the spherical pendulum [4] and which would allow correct uniform classical normalization and analysis at all values of  $\ell$ . It would be also interesting to develop the corresponding quantum description. The next step is combining this approach with the description of the two rotational degrees of freedom. Particularly interesting in this context is understanding the role of rotation and giving a complete assignment of the *ab initio* results in Ref. [22].

It is equally important to find the way of global analysis of the isomerizing triatomic molecules with pronounced stretching-bending Fermi resonance, such as HCP, HClO, etc. From the recent analysis of a similar model system, the 1:1:2 resonant “swing-spring” [26], we can expect that these molecules have nontrivial monodromy already in the limit of small oscillations about their stable equilibrium.

**ACKNOWLEDGMENTS**

We thank Boris Zhilinskiĭ and Richard Cushman for helpful discussions and comments on the manuscript. D.S. is grateful to the CNRS for making this work possible. D.S. and K.E. acknowledge the support by the EU network

project Mechanics and Symmetry in Europe (MASIE), Contract No. HPRN-CT-2000-00113.

**APPENDIX A: MATHEMATICAL BACKGROUND**

Since monodromy is relatively new to atomic and molecular physics, and furthermore, since it originated in integrable classical mechanical systems, we explain this concept here with an emphasis on its relation to approximately integrable (or Kolmogorov-Arnold-Moser) systems and corresponding quantum systems.

**1. A trivial example of global actions**

Recall that the Hamiltonian  $H$  of a  $K$ -dimensional non-resonant (and, in particular, nondegenerate) nonlinear oscillator can be put in the Birkhoff normal form  $\mathcal{H}(I_1, \dots, I_K)$ , which is a formal power series in actions of individual oscillators  $I_k = \frac{1}{2}(q_k^2 + p_k^2) \geq 0$  with  $k = 1, \dots, K$ . Clearly, the actions  $(I_1, \dots, I_K)$  are first integrals of the normalized system. For given nonzero values of actions, the trajectories of this latter system fill a particular  $K$ -dimensional torus.

The actions  $(I_1, \dots, I_K)$  can be easily quantized using the Bohr’s rule  $I_k = \hbar(n_k + \frac{1}{2})$  where the  $K$  quantum numbers  $n_k$  are non-negative integers and  $\hbar = 1$  in atomic units. Each quantum state is labeled uniquely by the set of quantum numbers  $(n_1, \dots, n_K)$ , and the (semiclassical) energy of the state is given by  $\mathcal{H}(n_1 + \frac{1}{2}, \dots, n_K + \frac{1}{2})$ . Recall also that the quantum wave function  $\psi_{n_1, \dots, n_K}(q_1, \dots, q_K)$  can be represented in the configuration space with coordinates  $(q_1, \dots, q_K)$  as a standing wave with  $n_k$  nodes in the direction  $q_k$ .

All classical and quantum states of the oscillator system in this example can be represented by points in a domain of a  $K$ -dimensional space  $\mathbb{R}^K$ , which is the image of the map  $I: \mathbb{R}^{2K} \rightarrow \mathbb{R}^K: (q, p) \rightarrow I(q, p)$ . The quantum states of this system form a lattice of points

(A1a)

whose “elementary cell” is defined by the way the quantum numbers label the states. A different choice of quantum numbers, for example,  $v_1 = n_1, v_2 = n_1 + n_2$ , corresponds to a different cell below.

(A1b)

Trivial as it may seem, the above combination of simple facts about the quantum-classical correspondence at the level of undergraduate quantum mechanics, has many ardent adherents among molecular physicists and theoretical chemists who use oscillator action-angle variables with considerable success in the analysis of molecular vibrations and other systems.

**2. Local action-angle variables**

Consider a Hamiltonian dynamical system with  $K$  degrees of freedom defined on a  $2K$ -dimensional phase space  $M$  with a Poisson structure  $\{\cdot, \cdot\}$ . Our system is *Liouville integrable* if we can find  $K$  independent Hamiltonian functions  $F = (F_1, \dots, F_K)$  which are mutually in involution, i.e., all Poisson brackets  $\{F_i, F_j\}$  vanish, and the Hamiltonian  $H$  of the system can be expressed as a function of  $(F_1, \dots, F_K)$ .

**a. Period lattice on regular tori**

If  $f = (f_1, \dots, f_K)$  is a regular (noncritical) value in the image of the integral map  $F: M \rightarrow \mathbb{R}^K$  defined by  $(F_1, \dots, F_K)$ , then by the Poincaré-Liouville-Arnol'd theorem [1–3], each compact connected component of the constant level set of first integrals  $(F_1, \dots, F_K)$  is a  $K$  torus  $\mathbb{T}_f^K$  in  $M$  characterized (labeled) by the values of integrals  $(f_1, \dots, f_K)$  and, of course, by constant energy  $h(f_1, \dots, f_K)$ .

The Hamiltonian vector field

$$X_{F_i} = (\{q_1, F_i\}, \dots, \{q_K, F_i\}, \{p_1, F_i\}, \dots, \{p_K, F_i\})$$

of each integral  $F_i$  in  $(F_1, \dots, F_K)$  defines a flow  $\varphi_{F_i}$  on the torus  $\mathbb{T}_f^K$  in  $\mathbb{R}^{2K}$ . The Hamiltonian flows  $(\varphi_{F_1}, \dots, \varphi_{F_K})$  are not necessarily periodic. We can, however, choose special new Hamiltonian functions  $(I_1(F), \dots, I_K(F))$  called *actions*, whose vector fields  $(X_{I_1}, \dots, X_{I_K})$  define  $K$   $2\pi$ -periodic flows on  $\mathbb{T}_f^K$  parametrized by conjugate *angle* variables  $(\phi_1, \dots, \phi_K)$ . We say that the vector fields  $(X_{I_1}, \dots, X_{I_K})$  define the period lattice on  $\mathbb{T}_f^K$ . This period lattice can be extended to an open small neighborhood  $D(f)$  of  $f$  which contains regular values  $f'$ . As a result, local action-angle variables can be defined for all regular tori  $\mathbb{T}_{f'}^K$  with  $f'$  in  $D(f)$ .

**b. EBK quantization, local quantum numbers**

Once the period lattice is defined for all  $f'$  in  $D(f)$ , we can find (semiclassical) quantum energies  $H(f')$  on the basis of the EBK quantization principle. Specifically, we look for such tori  $\mathbb{T}_{f'}^K$  on which the values of actions  $I_k(f')$  equal  $2\pi\hbar(n_k + \mu_k)$ , where *local quantum numbers*  $n_k > 0$  are non-negative integers and correction constants  $\mu_k$  are often called Maslov indexes. All simple principles of quantum-classical correspondence that we summarized in Appendix A1 can be now transferred to the present system restricted to the values  $f'$  in  $D(f)$ .

As in the simple examples (A1a) and (A1b), coordinates in  $D(f)$  can still be given by local actions which are smooth functions of the integrals  $F$ . However, we usually label quantum states *directly* by the expectation values  $\langle f \rangle$  of the integrals and we use these values as coordinates in  $D(f)$  (and globally in the whole image of the map  $F$ ). In such natural coordinates, the simple rectangular lattice (A1a) becomes smoothly distorted. The nodal patterns in the original configuration space with coordinates  $(q_1, \dots, q_K)$  become also more intricate since they now follow projections of the flow of Hamiltonians  $(I_1, \dots, I_K)$ .

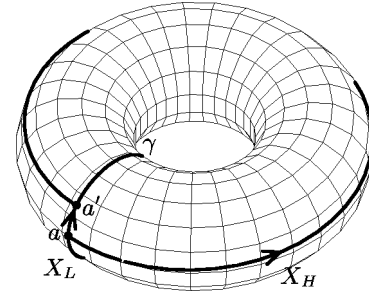


FIG. 14. The flow of the two vector fields  $X_H$  and  $X_L$  on a regular 2-torus  $\mathbb{T}_{(l,h)}^2$ ; the flow  $X_L$  is periodic while  $X_H$  is not.

**c. SO(2) symmetric systems with two degrees of freedom: Classical period lattice and quantum elementary cell**

In this paper, like in many of the initial studies of quantum and classical monodromy [7,8], we consider a special most simple situation where  $K=2$  and one of the integrals in  $F = (F_1, F_2)$  has a periodic flow. We will call this integral momentum  $L$ ; the flow of its Hamiltonian vector field  $X_L$  defines the Lie symmetry  $SO(2)$ . The other integral can be simply taken as the Hamiltonian  $H$  of the system, i.e., energy. The integral map  $F$  in this case is called the energy-momentum map  $\mathcal{EM}$ ,

$$\mathcal{EM}: \mathbb{R}_{q,p}^4 \rightarrow \mathbb{R}_{l,h}^2: (q,p) \rightarrow (L(q,p), H(q,p)),$$

where  $(q,p) = (q_1, p_1, q_2, p_2)$ ; the values of  $H$ ,  $L$ , and  $\mathcal{EM}$  will be denoted as  $h$ ,  $l$ , and  $(l,h)$ , respectively. The inverse image  $(\mathcal{EM})^{-1}(l,h)$  of point  $(l,h)$  is a *fiber* of the integrable foliation defined by  $F$ ; *singular* and *regular* fibers correspond to singular and regular values  $(l,h)$ . The rank of the  $2 \times 4$  matrix  $\partial(H, L) / \partial(q,p)$  equals 2 for all points  $(q,p)$  on regular fibers; it is less than 2 on some or all points of the singular fibers.

When the fibers are compact, then each connected component of a regular fiber  $(\mathcal{EM})^{-1}(l,h)$  is a 2-torus  $\mathbb{T}_{(l,h)}^2$ . Figure 14 illustrates defining the period lattice on  $\mathbb{T}_{(l,h)}^2$ . We take a periodic orbit  $\gamma$  of the flow of  $X_L$  and launch an orbit of the flow  $X_H$  from a point  $a \in \gamma$ . This orbit returns to  $\gamma$  at point  $a' \neq a$  after time  $T(l,h)$  called *period of first return*. As a coordinate on  $\gamma$  we use the angle  $\varphi_L \in [0, 2\pi)$  conjugate to  $L$ . The distance  $\Theta(l,h) = \varphi_L(a') - \varphi_L(a)$  between  $a$  and  $a'$  is called *rotation angle* or *rotation number*; it gives the “twist” of the flow  $X_H$ . The period lattice at  $a$  on  $\mathbb{T}_{(l,h)}^2$  has a basis  $\{X_{I_1}(a), X_{I_2}(a)\}$ , where

$$\begin{pmatrix} X_{I_1}(a) \\ X_{I_2}(a) \end{pmatrix} = A_{(l,h)}^\dagger \begin{pmatrix} X_L(a) \\ X_H(a) \end{pmatrix}. \tag{A2a}$$

Here we use the  $2 \times 2$  period lattice matrix

$$A_{(l,h)} = \frac{1}{2\pi} \begin{pmatrix} 2\pi & -\Theta(l,h) \\ 0 & T(l,h) \end{pmatrix}, \tag{A2b}$$

whose *columns* define the period lattice vectors. Neither the functions  $\Theta$  and  $T$  nor the basis depend on the choice of  $a \in \mathbb{T}_{(l,h)}^2$ .

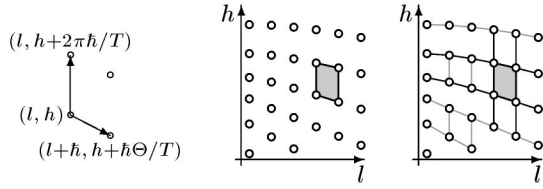


FIG. 15. Example of the local lattice of quantum states in a domain of the regular values of the energy-momentum map  $\mathcal{EM}$  of an  $\text{SO}(2)$  symmetric system with two degree of freedoms in Appendix A 2 c. Left panels show the initial “germ” cell; the right panel illustrates propagating this cell in order to define quantum numbers over a larger domain.

Rotation number  $\Theta(l, h)$  is a real *multivalued* function of  $(l, h)$ . However, we can always find a sufficiently small open neighborhood  $D(l, h)$  which consists of regular values of  $\mathcal{EM}$ , and where  $\Theta(l, h)$  can be defined uniquely so that, for example,  $0 \leq \Theta|_{D(l, h)} < 2\pi$ . This defines the period lattice (A2a) and (A2b) and locally over the whole  $D(l, h)$ . After integration, it also defines the corresponding actions  $(I_1, I_2)$  on  $D(l, h)$ .

Provided that the volume of  $D(l, h)$  is sufficiently large (compared to  $\hbar^2$ ), quantizing  $(I_1, I_2)$  produces a regular lattice of quantum states in  $D(l, h)$  illustrated in Fig. 15. The elementary cell of this lattice is related to the definition of the local period lattice in Eq. (A2a). To find the two basis vectors which define the cell as shown in Fig. 15, left, we step either  $n_1$  or  $n_2$  by 1 (so that the respective classical actions  $I_1=L$  and  $I_2$  step by  $\hbar$ ). Then in the first approximation

$$\begin{pmatrix} \Delta l \\ \Delta h \end{pmatrix} = (A_{(l, h)}^\dagger)^{-1} \begin{pmatrix} \Delta n_1 \\ \Delta n_2 \end{pmatrix} \hbar, \quad (\text{A3})$$

where the vectors are given by the columns of the inverse transpose matrix  $A_{(l, h)}$  times  $\hbar$ .

To verify Eq. (A3) note that local actions  $I_1$  and  $I_2$  are smooth functions of  $L(q, p)$  and  $H(q, p)$ ; in our case we can use  $I_1=L$ . The vector fields in Eq. (A2a) are

$$X_{I_1} = X_L, \quad X_{I_2} = \nabla I_2 \mathcal{J},$$

where

$$\nabla = \left( \frac{\partial}{\partial q_1}, \frac{\partial}{\partial q_2}, \frac{\partial}{\partial p_1}, \frac{\partial}{\partial p_2} \right), \quad \mathcal{J} = \begin{pmatrix} 0 & 0 & -1 & 0 \\ 0 & 0 & 0 & -1 \\ 1 & 0 & 0 & 0 \\ 0 & 1 & 0 & 0 \end{pmatrix}.$$

For  $I_2(L(q, p), H(q, p))$  we compute

$$X_{I_2} = \left( \frac{\partial I_2}{\partial L} \nabla L + \frac{\partial I_2}{\partial H} \nabla H \right) \mathcal{J} = \frac{\partial I_2}{\partial L} X_L + \frac{\partial I_2}{\partial H} X_H,$$

and consecutively

$$\begin{pmatrix} X_{I_1} \\ X_{I_2} \end{pmatrix} = \begin{pmatrix} 1 & 0 \\ \frac{\partial I_2}{\partial L} & \frac{\partial I_2}{\partial H} \end{pmatrix} \begin{pmatrix} X_L \\ X_H \end{pmatrix}.$$

Comparing this to Eq. (A2b) gives

$$-\frac{\Theta}{2\pi} = \frac{\partial I_2}{\partial L}, \quad \frac{T}{2\pi} = \frac{\partial I_2}{\partial H}.$$

To find the elementary cell of the quantum lattice, we can now use

$$\Delta I_2 = -\frac{\Theta}{2\pi} \Delta L + \frac{T}{2\pi} \Delta H, \quad \Delta I_1 = \Delta L,$$

or simply

$$(\Delta I_1, \Delta I_2) = (\Delta L, \Delta H) A_{(l, h)}.$$

Equation (A3) follows.

### 3. Defining global action-angle variables

We continue discussing the particular case introduced in Appendix A 2 c. The reader familiar with basic fiber bundle concepts has already noted that our map  $\mathcal{EM}$  defines a locally trivial 2-torus bundle over an open disk  $D(l, h)$  in  $\mathbb{R}^2$ . Indeed, local action-angle coordinates connect all fibers  $\mathbb{T}_{(l', h')}$  of this bundle with  $(l', h') \in D(l, h)$  so that locally the topology of the bundle is  $\mathbb{T}^2 \times D(l, h)$ . If global actions exist then the topology of the whole bundle is trivial. Below we discuss several less or more constructive ways of verifying this [27]. After reviewing the phenomenon of monodromy, we turn to our main objective—justifying the elementary cell method which we rely upon in the main body of the paper.

#### a. Analytic study of period lattices, monodromy

The method of analytic continuation of period lattices was detailed by Cushman [4,7]. Following the standard approach to uncovering topology of a fiber bundle, we define a closed loop  $\Gamma$  which passes through regular values  $(l, h)$  in the image of  $\mathcal{EM}$  (see Fig. 1). We take a point  $(l_0, h_0) \in \Gamma$ , define the period lattice as explained in Appendix A 2 c and Eq. (A2a) and (A2b), and then attempt to continue this period lattice for all consecutive points  $(l, h) \in \Gamma$  while moving along  $\Gamma$ . When we come back to the original point  $(l_1, h_1) = (l_0, h_0)$  of the loop, we compare the initial and final period lattices given by matrices  $A_{(l_0, h_0)}$  and  $A_{(l_1, h_1)}$ . If these lattices differ and

$$MA_{(l_0, h_0)} = A_{(l_1, h_1)},$$

where the monodromy matrix  $M$  is not unity, then the topology of the bundle is nontrivial and the actions we used to define our lattices are not global.

At the origin of monodromy is the possibility for the rotation number  $\Theta$  in Eq. (A2b) to jump by  $k2\pi$  after our tour on  $\Gamma$  so that at the end point we have



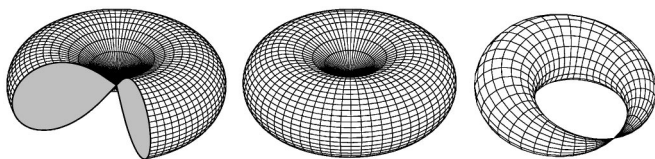


FIG. 16. Two possible plots of a pinched torus; cf. Chap. IV.3, Fig. 3.5 on p. 163 of Ref. [4]. Both representations are equivalent in the four-dimensional phase space.

$$\Theta(l_0, h_0) = \Theta(l_1, h_1) + k2\pi.$$

The matrix  $M$  does not depend on the choice of  $\Gamma$ , but depends, of course, on the choice of the basis. In the basis  $(X_{I_1}, X_{I_2})$  defined by the initial lattice  $A_{(l_0, h_0)}$  in Eq. (A2b), this matrix equals  $A^{-1}MA = \begin{pmatrix} 1 & -k \\ 0 & 1 \end{pmatrix}$ . We say that our system has monodromy  $k$ .

### b. Geometric monodromy theorem

Cushman and Duistermaat [28] proved that global action-angle variables over a punctured open disk  $D(0,0) \setminus (0,0)$  of regular values  $(l, h)$  of the  $\mathcal{EM}$  map do *not* exist if  $(0,0)$  is an isolated critical value of the  $\mathcal{EM}$  map which corresponds to the singular fiber called pinched torus. As shown in Fig. 16, this singular fiber is a torus with one basic cycle contracted to a point. The point is an unstable equilibrium of the system, while the rest of the fiber corresponds to the homoclinically connected stable and unstable manifolds of this equilibrium. Furthermore, for a contour  $\Gamma$  around  $(0,0)$ , monodromy computed as explained in Appendix A 3 a is 1 [29].

## APPENDIX B: SPHERICAL PENDULUM SYSTEMS

Spherical pendulum was discovered by Huygens about 30 years before Newton (see Ref. [4], p. 402). Some 360 years later, Duistermaat used spherical pendulum as an example when he introduced Hamiltonian monodromy in 1980 [6]. It was largely due to Cushman that molecular physicists understood the monodromy of this system and became interested in its molecular analog [30]. The closest analog, which they came up with very early, was a flexible triatomic molecule HAB, such as HCN, HCP, HClO, etc.

With all parameters scaled out, the unconstrained Hamiltonian of the spherical pendulum is

$$H = \frac{1}{2}(p_x^2 + p_y^2 + p_z^2) + z = \frac{1}{2}\mathbf{p}^2 + z. \quad (\text{B1a})$$

The motion is constrained to the surface of the sphere and the momentum vector is tangent to this surface,

$$\mathbf{r}^2 = x^2 + y^2 + z^2 = 1, \quad \mathbf{r} \cdot \mathbf{p} = xp_x + yp_y + zp_z = 0. \quad (\text{B1b})$$

This system is invariant with regard to rotations about axis  $z$ . The corresponding first integral is, of course, the  $z$  component of the angular momentum

$$L = [\mathbf{r} \wedge \mathbf{p}]_z = xp_y - yp_x. \quad (\text{B2})$$

Mathematical analysis of spherical pendulum can be found in Chap. IV of Ref. [4]. The leitmotiv there is “no polar coordinates.” We like to give an idea of why and how this is done without polar coordinates.

### 1. Energy-momentum map

We explain how to find the image and fibers of the  $\mathcal{EM}$  map of the spherical pendulum system (Fig. 1) directly from Eqs. (B1). Alternatively, this can be done after reducing the axial symmetry, see Appendix B 2 and Ref. [4].

The integral fibration of the spherical pendulum system defined in Eq. (B1) can be analyzed using the  $4 \times 6$  Jacobian matrix  $\partial F / \partial \xi$ , where  $F = (L, H, \mathbf{r}^2, \mathbf{r} \cdot \mathbf{p})$  and  $\xi = (x, y, z, p_x, p_y, p_z)$ . We compute the rank of this matrix. Specifically, we find all critical points  $\xi_c$  of  $F$  where this rank is less than 4 and then compute the corresponding critical values  $(L(\xi_{\text{crit}}), H(\xi_{\text{crit}}))$  of the  $\mathcal{EM}$  map.

#### a. Equilibria and relative equilibria

Critical values  $(0,1)$  and  $(0,-1)$  of the  $\mathcal{EM}$  map of the spherical pendulum system have rank 0 and correspond to the upper unstable equilibrium with  $z=1$  and the lower stable equilibrium with  $z=-1$ , respectively. Critical values with rank 1 lift to the *relative equilibria*, which are periodic trajectories coinciding with the orbits of the axial symmetry action, i.e., the orbits of the flow  $\varphi_L$  of the angular momentum  $L$  in Eq. (B2). They project to latitudinal circles in the configuration space  $S^2$  and correspond to the maximum length  $|L| = |\ell|$  at each given fixed energy  $h$ .

The study of  $\partial F / \partial \xi$  can be simplified if we use the axial symmetry of the system and restrict  $\partial F / \partial \xi$  to a vertical plane containing axis  $z$ , such as the plane  $\{x=0\}$ . Note that for relative equilibria  $\dot{z} = p_z = 0$ . Furthermore, when  $x = p_z = 0$  we can only satisfy Eq. (B1b) if either  $y=0$  or  $p_y=0$ . The former solution corresponds to the two equilibria with  $z = \pm 1$ ; we should, therefore, use the latter solution. Direct computation now shows that  $\partial F / \partial \xi|_{x=p_z=p_y=0}$  has only three  $4 \times 4$  minors with nonzero determinants:

$$D_1 = -zd, \quad D_2 = -yd, \quad D_3 = p_x d,$$

where  $d = y^2 + zp_x^2$ . The nontrivial solution of  $D_1 = D_2 = D_3 = 0$ ,

$$\ell = \pm (1 - z^2) / \sqrt{-z}, \quad h = (3z^2 - 1) / (2z), \quad (\text{B3})$$

where  $-1 < z < 0$  is the elevation of the relative equilibrium, leads to  $d=0$  and is compatible with Eq. (B1b) and  $x = p_z = p_y = 0$ . Equations (B3) define the relation between  $h$  and  $\ell$  for relative equilibria, and give the lower boundary of the image of the  $\mathcal{EM}$  map in Fig. 1.

#### b. Pinched torus

The critical value  $(\ell, h) = (0, 1)$  (see Fig. 1) corresponds to the upper equilibrium with  $z=1$  and all homoclinic orbits which begin and come back to this equilibrium (in infinite time) while zooming by the bottom point  $z=-1$  with just enough energy to climb back up. These trajectories fill up the

pinched torus shown in Fig. 16, center. To verify the topology of this singular fiber consider a section of  $\mathbb{R}^6$  by a half-plane  $\{x=0, y>0\}$ . Since  $L=0$  and  $y \neq 0$ , it follows that  $p_x = 0$ . Solving Eqs. (B1) with  $H=1$  gives the equation of the cusped circle

$$p_z^2 = 2(z-1)^2(z+1),$$

which is the section of the pinched torus with  $\{x=0, y>0\}$ . By axial symmetry all such sections are the same.

### c. Topology of the constant energy-level sets

All other values of  $\mathcal{EM}$  (represented in Fig. 1 by the gray shaded area) correspond to regular tori  $\mathbb{T}^2$ . Depending on the energy  $h$  these tori foliate the constant  $h$ -level sets in two different ways. Below  $h=1$ , regular tori are packed into a  $\mathbb{S}^3$ , while above  $h=1$  they form an  $\mathbb{R}P^3$  [4]. The former topology corresponds to the level set of the 1:1 resonant oscillator (a Hopf bifurcation), while the latter to a rotator. We speak of “vibrations” at  $h < 1$  and “rotations” for  $h > 1$  (when the pendulum goes over the top), cf. Sec. II A 2.

## 2. Reduction of axial symmetry

Physicists always reduce the axial symmetry of Eq. (B1) by introducing polar coordinates  $(\varphi, \theta)$ , where  $\varphi$  is the angle variable conjugate to  $L$ , see Ref. [31], Chap. III-14, problem 1. The downside of polar coordinates is their singularity at the linear equilibria of the system where  $\theta$  equals 0 or  $\pi$ . So the simplification comes at the price of losing correct geometry. In particular, it is difficult to work near the equilibria, to study their stability, etc. Furthermore, it becomes impossible to do standard classical normalization of molecular analog systems uniformly for all  $\ell$  [18,19]. Details of the geometrically correct reduction of the spherical pendulum system are presented in Ref. [4] and are summarized in Appendix B 2 b in order to give the idea of how troubles can be avoided.

### a. Reduction in polar coordinates

In polar coordinates, the reduced system with one degree of freedom describes the latitudinal motion in  $\theta$ ; the reduced Hamiltonian is

$$H_\ell = \frac{1}{2}p_\theta^2 + \frac{1}{2}\ell^2(\sin \theta)^{-2} - \cos \theta \quad \text{when } \ell \neq 0, \quad (\text{B4a})$$

$$= \frac{1}{2}p_\theta^2 - \cos \theta \quad \text{when } \ell = 0, \quad (\text{B4b})$$

where angle  $\theta$  is defined as shown in Fig. 3, and  $p_\theta$  is the corresponding conjugate momentum. Note that

$$J^2 = p_\theta^2 + \frac{\ell^2}{\sin^2 \theta} \quad (\text{B5})$$

is the square of the total angular momentum  $\mathbf{J}$  of the system and  $\ell$  is projection of  $\mathbf{J}$  on axis  $z$ .

Practitioners use physical intuition to compensate for the singularity of polar coordinates in Eq. (B4). Thus relative equilibria discussed in Appendix B 1 correspond to the equi-

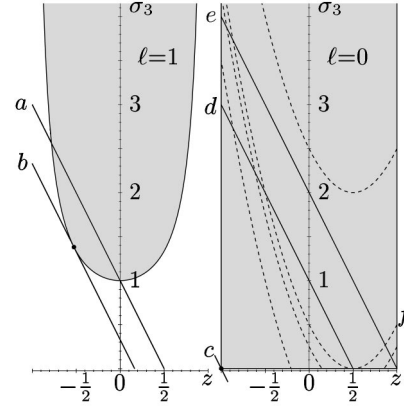


FIG. 17. The  $\{p_z=0\}$  plane projections of the reduced spaces (shaded area)  $P_{\ell=1}$  (left) and  $P_{\ell=0}$  (right), and of the  $h$ -level sets for the spherical pendulum (solid lines  $a, b, c, d, e$ ) and its quadratic deformation (dashed lines, label  $f$ ).

libria of the reduced system with Hamiltonian  $H_\ell$  for  $\ell \neq 0$  [see Eq. (B4a)] and are defined by the equations

$$\dot{\theta} = p_\theta = 0, \quad \dot{p}_\theta = \{p_\theta, H_\ell\} = -\partial H_\ell / \partial \theta = 0.$$

At the same time, the two equilibria with  $x=y=0$  correspond to the equilibria of the reduced system with  $\ell=0$  [use  $H_\ell$  in Eq. (B4b)].

### b. Reduction using polynomial invariants

Consider the action of the axial symmetry  $\text{SO}(2)$  on the six-dimensional space  $T\mathbb{R}^3$  with coordinates  $(\mathbf{r}, \mathbf{p}) = (x, y, z, p_x, p_y, p_z)$  generated by the flow  $\varphi_L$  of the system with Hamiltonian  $L$  in Eq. (B2). Six basic invariants,

$$z, \quad p_z, \quad L, \quad \sigma_3 = p_x^2 + p_y^2 + p_z^2,$$

$$\sigma_4 = x^2 + y^2, \quad \sigma_5 = xp_x + yp_y,$$

of this action can be used to express any  $\varphi_L$ -invariant function of  $(\mathbf{r}, \mathbf{p})$ . Taking constraints (B1b) into account (in other words, descending from  $T\mathbb{R}^3$  to the four-dimensional phase space  $\mathbb{T}\mathbb{S}^2$  of the spherical pendulum), we eliminate  $\sigma_4$  and  $\sigma_5$  and find that the reduced phase space  $P_\ell$  is a semialgebraic variety in  $\mathbb{R}^3$  defined by the equation and inequalities

$$p_z^2 + \ell^2 = \sigma_3(1 - z^2), \quad |z| \leq 1, \quad \sigma_3 \geq 0. \quad (\text{B6})$$

When  $\ell \neq 0$   $P_\ell$  is diffeomorphic to  $\mathbb{R}^2$ , but for  $\ell=0$  it is singular. Each point of  $P_\ell$  except for the two singular points with  $|z|=1$  of  $P_0$  lifts to circular orbits of  $\varphi_L$ ; the two  $|z|=1$  points lift to equilibrium points.

The reduced Hamiltonian  $H_\ell$  on  $P_\ell$  is

$$H_\ell(z, p_z, \sigma_3) = \frac{1}{2}\sigma_3 + z. \quad (\text{B7})$$

To determine the topology of the fibers of the  $\mathcal{EM}$  map we need to find intersections of  $P_\ell$  and constant  $h$ -level sets of  $H_\ell$ . Furthermore, since  $H_\ell$  and  $P_\ell$  are invariant with respect to “time reversal”  $p_z \rightarrow -p_z$ , we project in the plane  $\{p_z=0\}$ , see Fig. 17. In this plane, the  $h$  levels of  $H_\ell$  in Eq. (B7) become lines, and the  $h$  levels of the deformed spherical

pendulum parabolas, whose intersections with  $P_\ell$  can be easily found.

To reconstruct the fibers of  $\mathcal{EM}$  we lift the intersections  $a, b, c, d, e$ , shown in Fig. 17 to  $P_\ell$  and then back to the original phase space. Thus  $b$  and  $d$  are circles on  $P_\ell$ , which lift to tori  $\mathbb{T}^2$ ; the singular intersection  $e$  is a cusped circle which lifts to a pinched torus; one-point intersections lift to relative equilibria (RE) if the point is regular ( $a$  with  $|z| < 1$ ), and to an equilibrium point if the point is singular ( $c$  with  $|z| = 1$ ). Similar analysis can be done for the levels of the quadratic spherical pendulum (dashed lines in Fig. 17). In particular, section  $f$  is a figure eight curve on  $P_{\ell=0}$  which corresponds to the fiber shown in Fig. 6, left.

### 3. Quadratic aspherical pendulum

Quadratic deformation of the spherical pendulum is obtained after replacing  $z$  in Eq. (B1a) for a quadratic potential  $V(z)$  in Sec. II C. The energy-momentum relation

$$\ell(z) = \pm (1 - z^2) \sqrt{c_2 - \frac{c_1}{z}},$$

$$h(z) = c_0 + \frac{1}{2} \left( c_2 - \frac{c_1}{z} \right) + \frac{3}{2} c_1 z - c_2 z^2,$$

for the relative equilibria of this system can be obtained following the same approach as in Appendix B 1 a. However, now  $z$  takes three different types of values:  $z \in [-1, 0)$  for the lower stable RE ( $A$ ),  $z \in [c_1/c_2, z_c]$  for the unstable RE ( $X$ ), and  $z \in [z_c, 1]$  for the upper stable RE ( $B$ ).

The deformed system has only one essential parameter  $c = c_2/c_1$  which defines the ratio

$$(h_X - h_B)/(h_X - h_A) = (c - 1)^2/(c + 1)^2,$$

where  $h_X$  is the energy of the unstable RE at  $\ell=0$  (the ‘‘barrier’’), and  $h_A$  and  $h_B$  are energies of the two equilibria, see Fig. 5. For HCN/CNH and LiNC/NCLi we have  $c \approx 10.5$  and 3.8, respectively. Other parameters serve scaling and shifting the  $\mathcal{EM}$  characteristics.

The elevation  $z_c$  for the ‘‘cusp’’ points  $\alpha_\pm$  of the  $\mathcal{EM}$  diagram in Fig. 5 can be obtained by searching for the nontrivial common zeroes of  $dh/dz$  and  $d\ell/dz$ . In this way we find that  $z_c$  is the real root of  $1 + 3z^2 - 4cz^3 = 0$ . In the example of Sec. II C  $z_c = 0.361$ .

Deformation of the shape of the pendulum, i.e., of the surface on which the body is moving (Sec. II D), complicates the kinetic energy of the system. However, for relative equi-

libria where  $p_\theta = 0$  and  $\dot{\theta} = 0$ , only the change in the second term of  $H_\ell$  in Eq. (B4a) matters; this term becomes

$$T_\ell = \ell^2 [2mR(\theta)^2 \sin^2 \theta]^{-1},$$

where the mass  $m$  is used for scaling, and  $R(\theta)$  is given by Eq. (2) with  $R_0$  set to 1. Solving equations

$$\partial(T_\ell + V(\cos \theta))/\partial \theta = 0, \quad T_\ell + V(\cos \theta) = h,$$

for  $\ell(\zeta)$  and  $h(\zeta)$  where  $\zeta = \cos \theta$ , defines parametrically the energy-momentum characteristics of RE.

When  $\epsilon < \frac{1}{3}$ , i.e., when asphericity is *small*, the  $\mathcal{EM}$  map is qualitatively the same as for  $\epsilon = 0$  (Fig. 5). The  $\mathcal{EM}$  characteristics of  $A$ ,  $X$ , and  $B$  are now parametrized by  $\zeta$  on the intervals  $[-1, 0)$ ,  $[\zeta_1, \zeta_c]$ , and  $[\zeta_c, 1]$ , respectively. Here  $\zeta_1 \approx c^{-1} + c^{-1}(1 - c^{-2})\epsilon + O(\epsilon^2)$  is the real root of  $\epsilon c \zeta^3 + (1 - \epsilon)c \zeta - 1$ , such that  $\ell(\zeta_1) = 0$ . The cusp point is given by the real root  $\zeta_c \in (\zeta_1, 1)$  of

$$4c\zeta^3 - 3\zeta^2 - 1 - \epsilon(40c\zeta^5 - 27\zeta^4 - 32c\zeta^3 + 14\zeta^2 + 5) + O(\epsilon^2).$$

When  $\epsilon > \frac{1}{3}$  the solutions  $A$ ,  $B$ , and  $X$  are defined by  $\zeta$  in the intervals  $[-1, 0)$ ,  $[1, \zeta_0)$ , and  $[\zeta_1, 0)$ , respectively. Here  $\zeta_0 = \sqrt{1 - (3\epsilon)^{-1}}$  and  $\ell(\zeta_0) = \infty$ . These solutions are shown in Fig. 8 for the quadratic potential in Sec. II C, asphericity  $\epsilon = \frac{1}{2}$  and scaling  $m = 2.5$ .

The critical value of  $\epsilon = \frac{1}{3}$  has a simple geometrical explanation. At this value, the shape of the molecule given by Eq. (2) bifurcates so that at larger  $\epsilon$  it is no longer convex. To verify, note that the dent develops at  $\theta = \frac{1}{2}\pi$ , where  $z = R(\theta)\cos \theta = 0$ , and compute

$$\left( \frac{d}{dz} \right)_{z=0}^2 x = \left( \frac{d}{dz} \right)_{z=0}^2 R(\theta) \sin \theta = \frac{3\epsilon - 1}{(1 - \epsilon)^2}.$$

### 4. Quantum energy-level spectrum

The spectrum of the quantum spherical pendulum and similar systems is computed straightforwardly by diagonalizing the quantum Hamiltonian  $\hat{H} = \frac{1}{2}\hbar^2 \hat{J}^2 + V(\theta)$ , where for the spherical pendulum  $V(\theta) = -\cos \theta$ , in the standard basis of spherical harmonics  $Y_{j\ell}$ . Here  $j = 0, 1, \dots, j_{\max}$  and  $\ell = 0, \pm 1, \dots, \pm j$  are the quantum numbers for the angular momentum  $J$  and its projection  $J_z$ , and  $j_{\max}$  is taken sufficiently large to assure the convergence of the required lower energies, see Chap. IV-26 and the end of Chap. IV-29 in Ref. [32]. Note that the quantum analog of  $J^2$  in Eq. (B5) is

$$\hat{J}^2 = -\frac{1}{\sin \theta} \frac{\partial}{\partial \theta} \sin \theta \frac{\partial}{\partial \theta} - \frac{\ell^2}{\sin^2 \theta}. \quad (\text{B8})$$

[1] V.I. Arnol'd, *Mathematical Methods of Classical Mechanics*, 2nd ed., Graduated Texts in Mathematics Vol. 60, translated by K. Vogtmann and A. Weinstein (Springer-Verlag, New York, 1989) [original Russian ed. (Nauka, Moscow, 1974)].  
 [2] V.I. Arnol'd, V. V. Kozlov, and A. I. Neĭshtadt, *Mathematical*

*Aspects of Classical and Celestial Mechanics. Dynamical Systems III*, Encyclopedia of Mathematical Sciences Vol. 3 (Springer-Verlag, Berlin, 1988).  
 [3] N. N. Nekhoroshev, *Funkc. Anal. Priloz.* **28**, 3 (1994).  
 [4] R. H. Cushman and L. Bates, *Global Aspects of Classical In-*



- tegrable Systems* (Birkhauser, Basel, 1997).
- [5] N. N. Nekhoroshev, *Usp. Mat. Nauk* **24**, 2 (1969); *Trans. Mosc. Math. Soc.* **26**, 180 (1972).
- [6] J. J. Duistermaat, *Commun. Pure Appl. Math.* **33**, 687 (1980).
- [7] R. H. Cushman, *Cent. Wisk. Inform. Newsletter* **1**, 4 (1983).
- [8] R. H. Cushman and J. J. Duistermaat, *Bull., New Ser., Am. Math. Soc.* **19**, 475 (1988).
- [9] D. A. Sadovskii and R. H. Cushman, *Europhys. Lett.* **47**, 1 (1999); *Physica D* **142**, 166 (2000).
- [10] I. N. Kozin and R. M. Roberts, *J. Chem. Phys.* **118**, 10 523 (2003).
- [11] M. S. Child, T. Weston, and J. Tennyson, *Mol. Phys.* **96**, 371 (1999).
- [12] D. A. Sadovskii and B. I. Zhilinskii, *Phys. Lett. A* **256**, 235 (1999); L. Grondin, D. A. Sadovskii, and B. I. Zhilinskii, *Phys. Rev. A* **65**, 012105 (2001).
- [13] H. Waalkens, A. Junge, and H. R. Dullin, *J. Phys. A* **36**, L307 (2003).
- [14] S. Vũ Ngọc, *Commun. Math. Phys.* **203**, 465 (1999).
- [15] M. P. Jacobson and M. S. Child, *J. Chem. Phys.* **114**, 262 (2001).
- [16] J. N. Murrell, S. Carter, and L. O. Halonen, *J. Mol. Spectrosc.* **93**, 307 (1982).
- [17] J. M. Bowman, B. Gazdy, J. Bentley, T. J. Lee, and C. Dateo, *J. Chem. Phys.* **99**, 308 (1993).
- [18] D. Sugny and M. Joyeux, *J. Chem. Phys.* **112**, 31 (2000).
- [19] D. Sugny, M. Joyeux, and E. L. Sibert III, *J. Chem. Phys.* **113**, 7165 (2000).
- [20] M. Joyeux and D. Sugny, *Can. J. Phys.* **80**, 1459 (2002).
- [21] T. van Mourik, G. J. Harris, O. L. Polyansky, J. Tennyson, A. G. Császár, and P. J. Knowles, *J. Chem. Phys.* **115**, 3706 (2001).
- [22] G. J. Harris, O. L. Polyansky, and J. Tennyson, *Spectrochim. Acta, Part A* **58**, 673 (2002).
- [23] M. Joyeux, D. A. Sadovskii, and J. Tennyson, *Chem. Phys. Lett.* **382** 439 (2003).
- [24] R. Essers, J. Tennyson, and P. E. S. Wormer, *Chem. Phys. Lett.* **89**, 223 (1982).
- [25] G. Brocks and J. Tennyson, *J. Mol. Spectrosc.* **99**, 263 (1983); J. R. Henderson and J. Tennyson, *Mol. Phys.* **69**, 639 (1990).
- [26] H. Dullin, A. Giacobbe, and R. H. Cushman, *Physica D* (to be published).
- [27] We also like to draw attention to the geometric cycle basis approach to study monodromy and generalized definition of monodromy which was recently suggested by N. N. Nekhoroshev, D. A. Sadovskii, and B. I. Zhilinskii, *C. R. Acad. Sci., Ser. I: Math.* **335**, 985 (2002).
- [28] R. H. Cushman and J. J. Duistermaat, *J. Diff. Eqns.* **172**, 42 (2001).
- [29] The theorem in Ref. [28] extends to singular tori with  $k$  pinches using the result by N. Tien Zung, *Diff. Geom. Applic.* **7**, 123 (1997); *Lett. Math. Phys.* **60**, 87 (2002). In such case monodromy is  $k$ .
- [30] Applications of monodromy in molecules were first discussed by physicists and mathematicians at the joint Workshop, Non-linear Dynamics and Spectra (unpublished), organized by M. Roberts at the Mathematics Institute, Warwick University, UK, 1997. Discussions were initiated by M. Child and B. Zhilinskii after the talk by R. Cushman.
- [31] L. D. Landau and E. M. Lifshitz, *Mechanics*, 4th ed., Theoretical Physics, Vol. I (Nauka, Moscow, 1988), in Russian; *Mécanique* (Mir, Moscou, 1982), in French.
- [32] L. D. Landau and E. M. Lifshitz, *Quantum Mechanics. Non-Relativistic Theory*, 3rd ed. Theoretical Physics Vol. III (Moscow, Nauka, 1974), in Russian [English translation (Pergamon Press, Oxford, 1965)].